CHEMISTRY OF MATERIALS

pubs.acs.org/cm

Article

Tunable Sulfur Incorporation into Atomic Layer Deposition Films Using Solution Anion Exchange

Julia D. Lenef, Andrew J. Gayle, Jaesung Jo, Kalyn M. Fuelling, Srinivas K. Yadavalli, Alondra M. Ortiz-Ortiz, Kai Sun, Rebecca L. Peterson, and Neil P. Dasgupta*

Cite This: *Chem. Mater.* 2023, 35, 2503−2517

Read Online

ACCESS | Metrics & More | Article Recommendations | Supporting Information

ABSTRACT: Metal sulfide and oxysulfide thin films deposited by atomic layer deposition (ALD) are important functional materials for a range of applications including solar cells, catalysts, and electronic devices. However, ALD of sulfur-containing films typically requires H_2S, a toxic, corrosive, and flammable gas. To circumvent these challenges, we propose a method of tuning sulfur incorporation into ALD films by first growing a metal oxide, using CuO_x as a model system, followed by a solution-phase sulfur anion-exchange process. By controlling the reaction time, solution molarity, and temperature, we demonstrate tunable sulfur incorporation into the films, which is described using a coupled reaction-diffusion model. The evolution of the film crystallinity, composition, and morphology was quantified as a function of the anion-exchange process parameters. Conformal anion exchange on a $ZnO@TiO_2@CuO$ core−shell−shell nanowire is shown, demonstrating the ability to maintain the conformality of the initial ALD process on high-aspect-ratio structures. Additionally, area-selective anion exchange was performed on micro-patterned substrates, illustrating a pathway toward device fabrication. Finally, the electrical properties of the converted films were evaluated, indicating a tunable reduction in sheet resistance of up to 4 orders of magnitude. In the future, the combination of ALD and anion-exchange chemistry can be used to incorporate sulfur without the need for H_2S gas, while maintaining the atomically precise and conformal properties of the original ALD process.

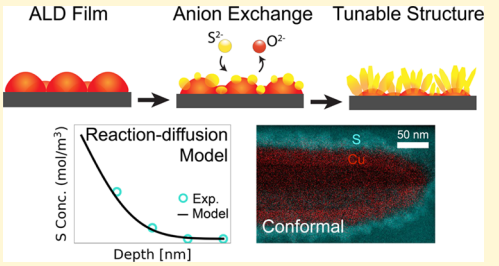

INTRODUCTION

Metal sulfides and oxysulfides are important functional materials in numerous applications including batteries,[1,2] photocatalysts,[3] electrocatalysts,[4,5] sensors,[6] solar cells,[7] and thin-film transistors (TFTs).[8] Atomic layer deposition (ALD) is an important technique to synthesize metal sulfides with sub-nanometer thickness control, while facilitating unparalleled conformality and uniformity over nonplanar surface geometries.[9,10] These characteristics motivate the increasing use of ALD in applications where conventional physical vapor deposition, chemical vapor deposition, or solution processing are not sufficient.

The synthesis of sulfide films by ALD typically requires H_2S, which is a toxic, corrosive, and flammable gas.[11] In addition to safety considerations, the use of H_2S gas also requires modification to ALD reactor hardware to ensure chemical compatibility.[12] As an alternative, elemental sulfur[13] and organosulfur compounds[14,15] have been explored to avoid the use of H_2S, but these sulfur precursors suffer either from reduced volatility or fewer demonstrations of self-limiting processes. Therefore, H_2S remains the dominant precursor that is used for metal sulfide ALD, motivating further research to develop new processes for conformal and tunable metal sulfide and oxysulfide layers.[11]

One approach to avoid the use of H_2S gas is to grow the initial oxide by ALD followed by a secondary reaction with a non-H_2S sulfur source. Previous demonstrations of this approach in the literature have reported postannealing of the ALD metal oxide in the presence of an elemental sulfur solid[16−19] or CS_2 gas.[20] However, the sulfurization process relies on high temperatures (>300 °C), which may limit its application when the process is performed on thermally sensitive substrates such as electronic devices and polymers. Additionally, the generation of sulfur vapor may cause undesirable contamination and/or compatibility issues.

To address these limitations, in this study, we demonstrate a solution-phase sulfur anion-exchange process to facilitate tunable incorporation of sulfur into ALD oxide films. This process can be performed at room temperature, is compatible with photolithographic patterning, and maintains the inherent conformality of existing ALD oxide processes on 3D templates. Previous work has demonstrated that cation-exchange

Received: December 21, 2022
Revised: March 5, 2023
Published: March 17, 2023

Scheme 1. Conceptual Illustration of the Solution-Phase Sulfur Anion-Exchange Process into CuO_x ALD Thin Films[a]

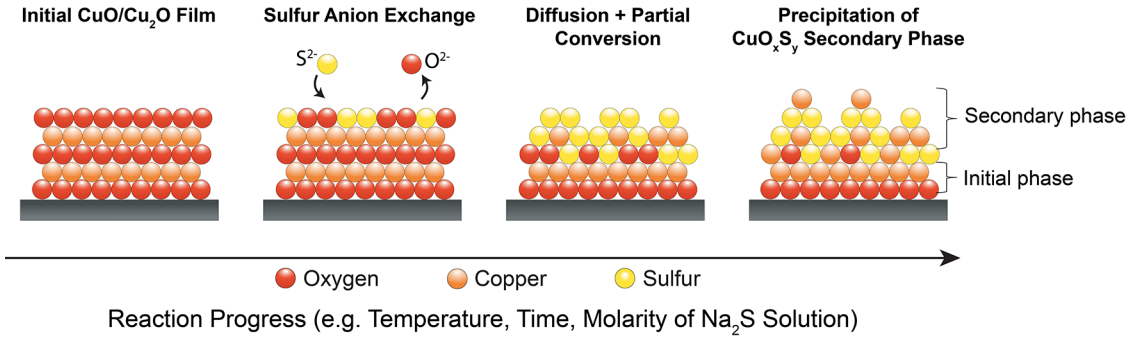

[a]After sulfur anion exchange, structural rearrangement occurs due to the interdiffusion of atomic species and precipitation of a CuO_xS_y (secondary) phase, which grows on the surface. The rate and extent of sulfur incorporation into the underlying film (i.e., initial phase) can be tuned by the solution molarity, temperature, and time.

reactions can occur in the gas phase during the ALD process, allowing for conversion of ZnS and Cu_2S phases.[21] Furthermore, solution-phase cation-exchange reactions have been previously demonstrated on ALD ZnO layers to form FeOOH on graphene nanosheets.[22] In addition, chalcogenide-based anion exchange was implemented to produce ZnSe, which was followed by cation exchange to form CdSe on inverse opal structures.[23] However, the current study is the first report to date of solution-phase sulfur anion-exchange chemistry of any ALD film.

To facilitate the anion-exchange process, the solubility product constant (K_{sp}) of the resulting metal sulfide should be significantly lower than the initial metal anion (typically oxide) film, which is true for numerous metal oxides.[24−26] To demonstrate the feasibility of sulfur anion-exchange chemistry in ALD films, in this study, we used CuO and Cu_2O as model starting systems. Both of these oxide phases, and the associated family of copper sulfides (e.g., CuS and Cu_2S), are typically p-type semiconductors, facilitating their use in a wide range of applications such as solar cells,[27−29] thin-film transistors[30−32] and photo- and electrocatalysis.[3,33,34] In particular, the integration of sulfur into copper oxides has been previously explored to form copper oxysulfides,[35] modify the oxide surface with CuS layers,[3,36−38] or provide doping-level sulfur content.[39,40] In the case of CuO_xS_y alloys, experimental[35] and computational[41] evidence suggests that control over the structural, optical, and electronic properties of the semiconductor can be achieved by tuning the sulfur content in the copper oxide host material. Therefore, there is a strong motivation to apply sulfur anion exchange for both complete sulfur/oxygen exchange throughout the entire film, as well as partial exchange of anions on the ALD film surface.

To facilitate partial exchange of an oxide film into an oxysulfide, there is a need for an improved mechanistic understanding of the anion-exchange process, which could enable rational design of the resulting material structure and properties. For example, enabling improved control of partial ion exchange reactions can be useful for tuning the surface structure, electrical properties, band alignment, and optical transparency. However, to date, there have been relatively few studies[24,42−44] that explore the influence of solution anion-exchange process conditions to control the structure, composition, and phase evolution during partial conversion of thin films. Furthermore, there have been no previous studies on partial solution anion exchange of ALD films.

In this study, we perform anion exchange on CuO and Cu_2O ALD films using aqueous solutions of sodium sulfide nonahydrate ($Na_2S{\cdot}9H_2O$), resulting in tunable incorporation of sulfur into the original ALD films (Scheme 1). In Scheme 1, we provide a simplified representation of the anion-exchange process, which involves diffusion, atomic rearrangement, and precipitation of a secondary phase. We note that the anion-exchange process presented in this work is not a pure topotactic anion exchange. The resulting CuO_xS_y solid can be described as a nanocomposite, since two or more phases may coexist within the structure after anion exchange. Therefore, this should not be viewed as a replacement to ALD of metal oxysulfides, but rather as a complementary method to incorporate sulfur into ALD surfaces.

We demonstrate the ability to control the degree of sulfur-to-oxygen anion exchange by varying the process parameters including reaction time, temperature, and solution molarity. The surface roughness, morphology, phase, and sheet resistance of the resulting nanocomposite were measured as a function of the anion-exchange process parameters. A reaction-diffusion model was developed, which enables predictive control of the anion-exchange process. Proof-of-concept anion-exchange conversion of a core−shell−shell nanowire formed by ALD was demonstrated, illustrating the feasibility of this technique to modify high-aspect-ratio geometries, while maintaining the inherent conformality of the original ALD film. In addition, area-selective anion exchange was demonstrated on a lithographically patterned film, providing a pathway toward device fabrication. In the future, the ability to rationally control and pattern anion-exchange processes will provide a versatile platform for simple, safe, and controllable sulfur incorporation into ALD films.

EXPERIMENTAL METHODS

ALD of Copper Oxide Starting Materials. Copper oxide thin films with tunable phase and composition were synthesized on Si wafers using a combination of plasma-enhanced ALD (PE-ALD) and post-deposition annealing. Further details of the ALD CuO_x process, including post-deposition annealing, can be found in our previous report.[45] To form phase-pure CuO, 300 W O_2 plasma was utilized as the oxidant with copper(I) *N*,*N*′-disec-butylacetamidinate ($[Cu(^sBu\text{-}amd)]_2$) as the metal precursor. The Cu precursor pulse time was 1.5 s, the O_2 plasma exposure time was 6 s, and the purge time was 8 s. The as-deposited film thickness was ∼30 nm, as measured by spectroscopic ellipsometry, with a growth rate of ∼0.3 Å/cycle. To convert the as-deposited CuO film into Cu_2O, annealing at a

https://doi.org/10.1021/acs.chemmater.2c03773
Chem. Mater. 2023, 35, 2503−2517

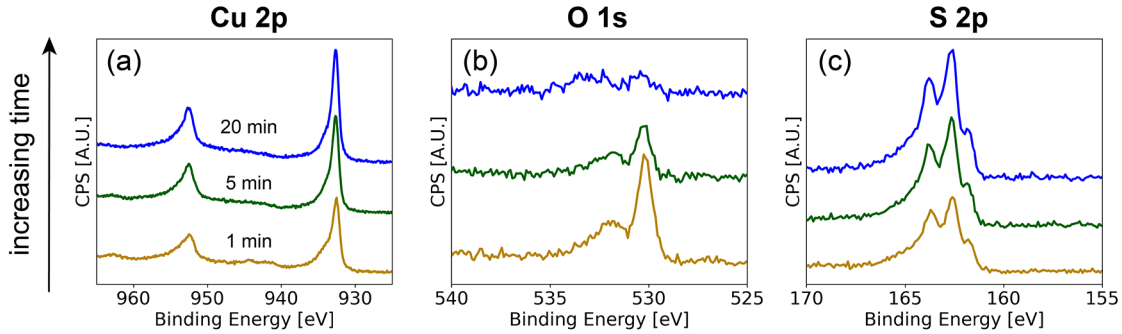

Figure 1. XPS core scans of sulfur-treated CuO thin films. (a) Cu 2p, (b) O 1s, and (c) S 2p core scans are shown for films treated using 0.5 mM Na_2S at RT after 1, 5, and 20 min of sulfur treatment. Surface scan, no Ar^+ sputtering applied.

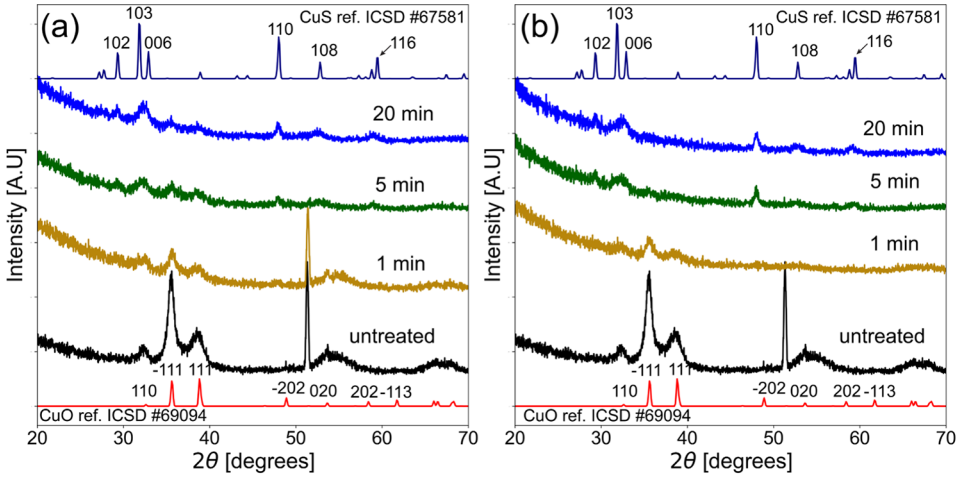

Figure 2. Benchtop GIXRD spectra of untreated and sulfur-treated ALD CuO films on Si substrates. A solution molarity of 0.5 mM was used, with reaction times of 1, 5, and 20 min at temperatures of (a) RT and (b) 80 °C. The sharp peak at 50.2° is attributed to the Si substrate.

temperature of 600 °C was performed in vacuum at 1×10^{-5} Torr. To deposit CuO thin films on ZnO nanowires, a recipe with longer exposures (3 s Cu precursor pulse and a 10 s O_2 plasma exposure separated by 8 s purge steps) was used to ensure conformal coverage.

Solution Anion Exchange. Sodium sulfide nonahydrate was ($Na_2S{\cdot}9H_2O$) purchased from Sigma-Aldrich (CAS: 1313-84-4). Aqueous solutions were prepared using deionized (DI) water with molarities of 0.05, 0.1, 0.25, and 0.5 mM with pH values less than ~10.5. Solution anion exchange of the initial CuO_x films was performed at both room temperature (RT) and 80 °C. Samples were inserted into the solution for controlled times spanning from 1 to 20 min. All samples were thoroughly rinsed with DI water after removal from the sulfur solution prior to further analysis.

Anion exchange on ZnO nanowires coated with ALD CuO shells was performed for 1 min using 0.5 mM Na_2S at 80 °C. A 5 nm TiO_2 interlayer was deposited between the ZnO nanowire and CuO film to prevent the diffusion and reaction of sulfur into the ZnO core. Details of the procedure for hydrothermal synthesis of ZnO nanowires[46] and the deposition of the TiO_2 diffusion barrier layer can be found in Supporting Note 1.

To demonstrate area-selective anion exchange, photolithographic patterning was performed. After patterning the polymeric photoresist, area-selective anion exchange was performed in the exposed areas of the substrate. After sulfur treatment, the photoresist layer was removed by soaking in acetone.

Materials Characterization. Phase analysis was performed using grazing-incidence X-ray diffraction (GIXRD). Benchtop GIXRD was performed using a Rigaku SmartLab X-ray diffractometer with a 2θ range of 20−70° and incident angle of 0.5−1°. Synchrotron GIXRD was performed at beamline 33-BM-C at the Advanced Photon Source (APS) at Argonne National Laboratory. The incident angle was fixed at 3° using a 1.5 keV X-ray energy (0.826 Å) and a 2θ range of 25−50°. The film thicknesses were evaluated by spectroscopic ellipsometry (J.A. Woollam M-2000). The data were fit using the BSpline model and the J.A. Woollam CompleteEASE software. The morphology and surface roughness were investigated by atomic force microscopy (AFM) collected on a Veeco Dimension Icon AFM in PeakForce Tapping mode. To evaluate the material composition, X-ray photoelectron spectroscopy (XPS) was performed on a Kratos Axis Ultra XPS with a monochromatic Al source (10 mA, 12 kV). Pass energies of 160 and 20 eV were used for the survey scans and the core scans, respectively. The XPS spot size was 700 μm × 300 μm and the spectra were calibrated to the C−C component of C 1s at 284.8 eV. Ar^+ sputtering was performed to evaluate the composition with respect to depth. One min of Ar^+ sputtering corresponds to a removal of ~7.5 nm in depth. Survey scans of as-deposited CuO and the resulting Cu_2O after post-deposition annealing revealed no detectable C and N from the Cu(I) amidinate precursor prior to exposure to the sulfur solution (Figure S1). High-angle annular dark-field scanning transmission electron microscopy (HAADF-STEM) images were collected on a Thermo Fisher Talos F200X G2 scanning/transmission electron microscope (S/TEM) with 200 keV accelerating voltage. Electron energy loss spectroscopy (EELS) was used to obtain elemental maps of the core−shell−shell nanowire sample. Scanning electron microscopy (SEM) images were collected using the TESCAN RISE and energy-dispersive X-ray spectroscopy (EDS) line scans and mapping were each performed at 5 keV, selected to allow for measurement of the characteristic Kα X-rays from sulfur. A low-pass filter was used for noise reduction.

Electrical Characterization. To prepare samples for sheet resistance measurements, CuO_xS_y layers were synthesized on boro-aluminosilicate glass substrates. Metal contacts of Ni/Au, with a

https://doi.org/10.1021/acs.chemmater.2c03773
Chem. Mater. 2023, 35, 2503−2517

thickness of 20/80 nm, were deposited by e-beam evaporation through a shadow mask. A van der Pauw configuration was used, with contacts at the four corners of a square sample. Four-point probe measurements were made in the dark at RT in air using an HP4156A semiconductor parameter analyzer.

RESULTS AND DISCUSSION

Sulfur Anion Exchange of ALD CuO Films. *XPS Analysis.* In this study, the sulfur anion-exchange process (Scheme 1) was performed on both phase-pure CuO and Cu_2O ALD thin films. We first describe the results when CuO was the initial phase. XPS analysis was performed to study the surface chemistry of the CuO films after the anion-exchange process. Figure 1a–c shows the core scans for Cu, O, and S using a 0.5 mM Na_2S solution at a temperature of RT, with varying reaction times (the initial CuO surface is shown in Figure S2). As the reaction time increases, we observe a reduction in the intensity of the O 1s peak (Figure 1b), and a corresponding increase in the S 2p intensity (Figure 1c). The asymmetric tail of the S 2p region and the presence of three distinct peaks are both common features found in the covellite phase (i.e., CuS).[47,48] In the O 1s spectra, we note that the primary peak, which is positioned at 530.2 eV, is associated with Cu–O bonding[49] (Figure 1b) while the secondary peaks at ~532 eV are attributed to organic species containing oxygen from adventitious surface carbon.[50] The decrease in the oxygen signal and the corresponding increase of sulfur indicate that the anion-exchange reaction was successful. Furthermore, the Cu 2p spectra remain largely unchanged, except for a decrease in the satellite peaks located at ~943 and ~963 eV (Figure 1a). These satellite peaks are associated with the presence of Cu^{2+} in the initial CuO phase (Figure S2), which are typically absent in copper core spectra for CuS_x phases, providing an additional signal of the successful anion-exchange process.[51]

GIXRD Analysis. Phase analysis after anion exchange of ALD CuO films was performed using GIXRD analysis. Benchtop GIXRD was performed on all samples, while a subset was analyzed by synchrotron GIXRD to provide further resolution. Figure 2a shows the benchtop GIXRD spectra of CuO films that were exposed to a 0.5 mM solution of Na_2S at RT for 1, 5, and 20 min time intervals. After 1 min of anion exchange, the CuO (110), (−111), and (111) peaks decreased in intensity compared to the as-deposited (untreated) CuO films. This indicates that the sulfur exchange process has started to disrupt the long-range ordering of the original CuO film surface, but the underlying CuO film remains intact (Scheme 1). Further evidence of this compositionally graded structure with partial conversion at the top surface will be described in detail in the following sections.

After anion exchange for 5 and 20 min at RT, peaks associated with the crystalline CuS phase emerged (Figure 2a), as evidenced by the (102) diffraction peak and a broad peak spanning the (103) and (006) peaks, along with the emergence of the (110), (108), and (116) peaks. The emergence of the crystalline CuS phase was further confirmed using synchrotron GIXRD analysis (Figure S3). When a higher temperature (80 °C) anion-exchange solution was used, benchtop GIXRD revealed the dominant phase to be CuS after 5 and 20 min of conversion (Figure 2b). However, when using synchrotron GIXRD after 20 min of conversion, very minor CuO (−111) and (111) peaks were still detectable (Figure S3). This demonstrates that an elevated solution temperature produced a more rapid conversion of the CuO to CuS, which can be attributed to a combination of faster interfacial-exchange kinetics and faster solid-state diffusion within the film.

Proposed Mechanism for Sulfur Anion Exchange of CuO Films. Based on the XPS and GIXRD analysis presented above, we propose the following possible reaction mechanisms for the conversion of CuO to CuS

$$CuO + S^{2-} + H_2O \rightarrow CuS + 2OH^- \quad (1)$$

$$CuO + HS^- \rightarrow CuS + OH^- \quad (2)$$

Analogous reactions to eq 1 have been previously proposed for various metal oxide films using Na_2S as the sulfur source.[26,52] Furthermore, because HS^- is also present in the aqueous Na_2S solution,[53] reaction 2 is an additional plausible pathway for the formation of CuS, which may be occurring concurrently with reaction 1.

We further investigated the effect of solution temperature and reaction time on the resulting surface morphology and roughness using AFM. Prior to sulfur treatment, the as-deposited CuO films have a root mean square (RMS) surface roughness of 2.3 nm with average grain sizes of 17.6 ± 3.5 nm (Figure S4). In general, as the film is exposed to longer sulfur treatment times, the surface roughness increases and vertical "platelets" grow out of the plane, which is a distinct morphology that has been observed previously for CuS synthesized by solution chemistry.[54,55] For example, as shown in Figure 3a–c, at RT after 1 min, the RMS surface roughness was 13.8 nm, which increased to 32.9 nm after 20 min. For applications where a high surface area and complex nanostructures are preferable (e.g., battery electrodes, catalysis) these features may be desirable, whereas in thin-film electronic devices, optimizing these conditions to minimize the changes in surface roughness may be necessary. Therefore, it is important to study the process-structure relationships that enable tunable control of the resulting surface morphology after anion exchange.

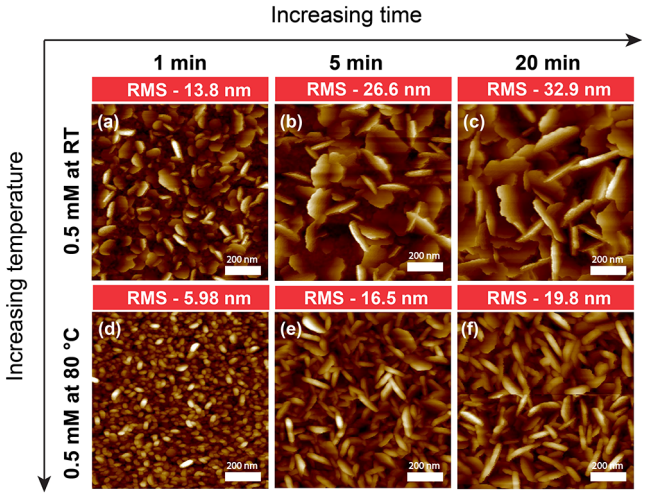

Figure 3. AFM images of CuO films following anion exchange using a Na_2S solution molarity of 0.5 mM. Treatments were performed either at RT for (a) 1 min, (b) 5 min, and (c) 20 min or at 80 °C for (d) 1 min, (e) 5 min, and (f) 20 min.

To demonstrate the ability to further tune the surface morphology during anion exchange, we studied the influence of solution temperature. Compared to the RT reaction

https://doi.org/10.1021/acs.chemmater.2c03773
Chem. Mater. 2023, 35, 2503–2517

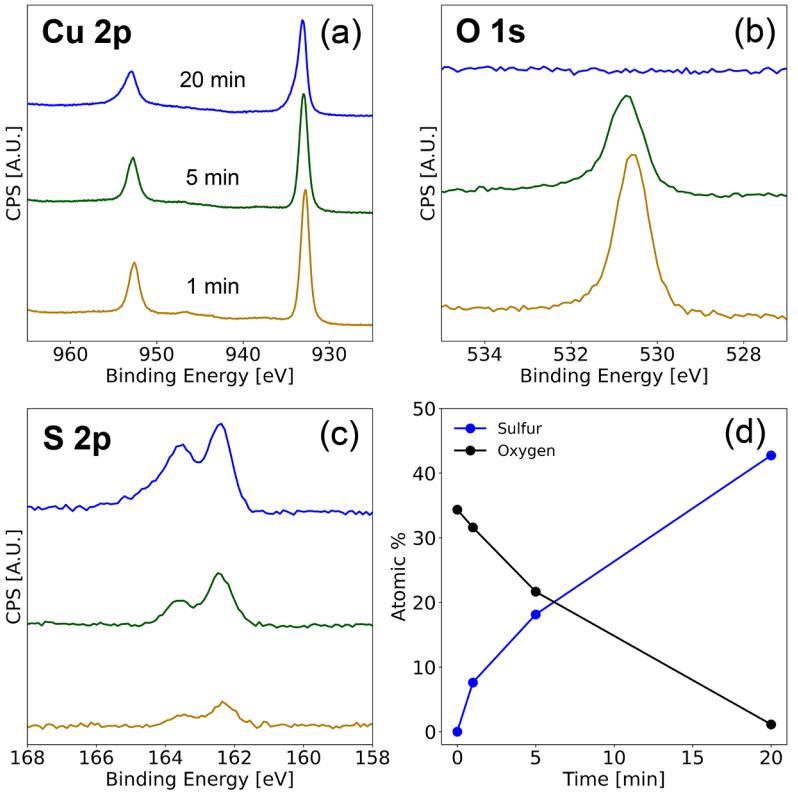

Figure 4. XPS core scans of sulfur-treated Cu_2O thin films. (a) Cu 2p, (b) O 1s, and (c) S 2p scans of films treated using 0.25 mM Na_2S at RT after 1, 5, and 20 min of sulfur treatment. (d) Atomic percentages of S and O as a function of the sulfur treatment time. Untreated S and O content is included for reference. All spectra were collected after 1 min of Ar^+ sputtering, and thus no surface O was observed.

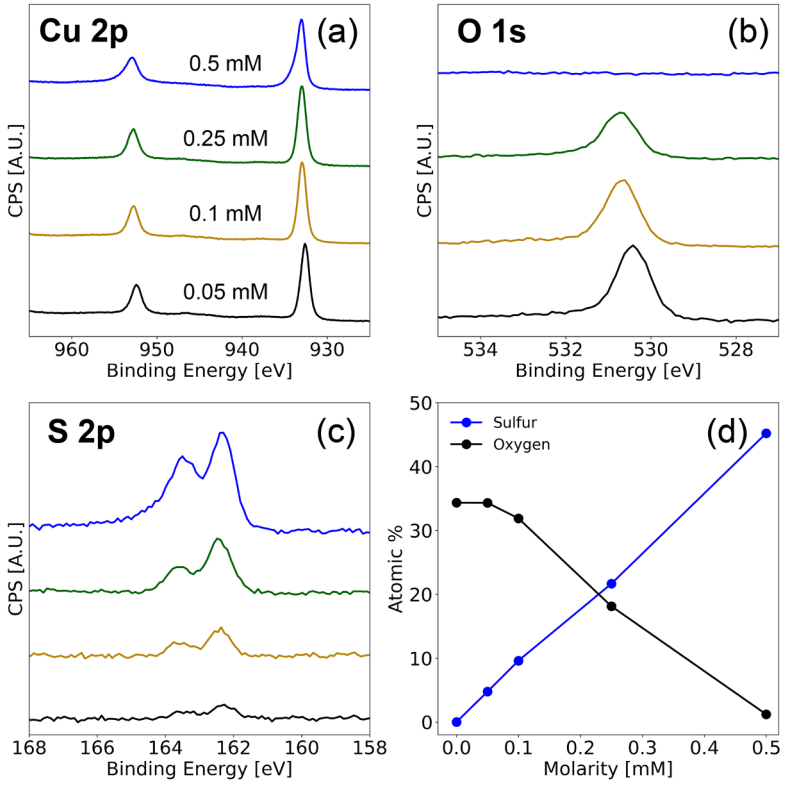

Figure 5. XPS core scans of sulfur-treated Cu_2O thin films. (a) Cu 2p, (b) O 1s, and (c) S 2p scans of films treated using various Na_2S solution molarities at RT for 5 min. (d) Atomic percentages of S and O as a function of Na_2S solution molarity. Untreated S and O content is included for reference. All spectra were collected after 1 min of Ar^+ sputtering, and thus no surface O was observed.

https://doi.org/10.1021/acs.chemmater.2c03773
Chem. Mater. 2023, 35, 2503−2517

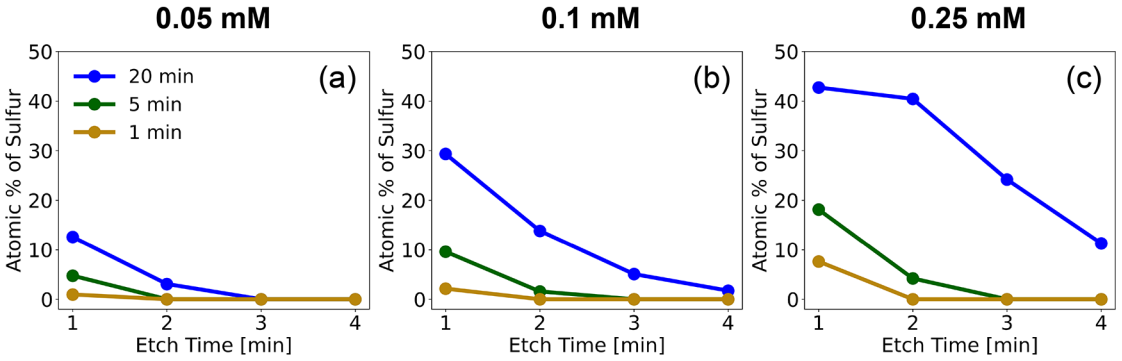

Figure 6. Sulfur composition via XPS with respect to depth (Ar^+ etch time) of Cu_2O thin films treated with Na_2S at RT. The time in solution was varied, and the Na_2S solution molarities were (a) 0.05 mM, (b) 0.1 mM, and (c) 0.25 mM. At a 3 min etch time, Si is detected, indicating that the SiO_2 substrate surface is reached.

condition (Figure 3a–c), when the solution temperature was increased to 80 °C (Figure 3d–f), the surface roughness was observed to increase more gradually. For example, after 20 min at RT, the RMS surface roughness was 32.9 nm while at 80 °C it was 19.8 nm (Figure 3c,f). Furthermore, the areal density of "platelets" is observably higher for the 80 °C reaction condition compared to synthesis at RT. This illustrates the ability to tune surface microstructure and morphology through rational control of the anion-exchange process parameters, which provides a process "knob" for the design of optimized material properties.

Sulfur Anion Exchange of ALD Cu_2O Films. *XPS Analysis.* In addition to experiments using CuO as the initial film composition, we also explored the sulfur anion-exchange process using Cu_2O films, which were formed by high-temperature vacuum annealing (i.e., 600 °C at 1×10^{-5} Torr) of the as-deposited ALD CuO films. We have previously demonstrated that these post-deposition annealing conditions can produce phase-pure Cu_2O from films with an initial phase of CuO.[45] We note that when a solution temperature of 80 °C and a molarity of 0.5 mM were used for the anion-exchange process, significant cracking and delamination of the Cu_2O thin film was observed after 2 min (Figure S5). Therefore, we focus on RT conditions when the initial phase was Cu_2O, to mitigate issues with mechanical degradation.

To characterize surface chemistry and chemical composition profile after anion exchange, XPS analysis was performed on the sulfur-treated samples after Ar^+ sputtering. Figure 4a–d shows the effect of anion-exchange time on the bonding environment of Cu, O, and S. As the Na_2S treatment time increases, a corresponding reduction in the O 1s peak intensity is observed (Figure 4b), which completely disappears after 20 min. Concurrent with the continual removal of oxygen from the film during extended reaction times, there is a gradual increase in the S 2p peak (Figure 4c). As a result of this sulfur incorporation into the film, a doublet peak is observed, which supports the presence of a Cu_2S bonding environment.[47,48] As a reference, the Cu 2p and O 1s core scans of the untreated initial Cu_2O film can be found in Figure S6.

Interestingly, when the reaction time is further increased at a sufficiently high molarity (e.g., 20 min at 0.25 mM, Figure 4d), the sulfur stoichiometry increases beyond Cu_2S. Figure 4d illustrates the inverse relationship between the oxygen and sulfur content with respect to the reaction time. After a 20 min reaction time, the atomic percentage of sulfur on the surface is greater than 40%. This suggests that sulfurization of the film continues beyond a 1:1 anion exchange of sulfur and oxygen, which will be discussed in further detail below. Further evidence of this continued sulfurization is observable in the asymmetric tail of the S 2p spectrum when the reaction conditions were 0.25 mM for 20 min, which is analogous to what was observed when the initial film phase was CuO (Figure 1c). The presence of this tail suggests that bonding environments such as Cu_7S_4 or CuS can form during extended sulfurization of the films, beyond the 1:1 anion exchange of sulfur for copper.[47,48]

In addition to increasing the reaction time, we also examined the influence of increasing solution molarity on the anion exchange of Cu_2O films, when the reaction time was held constant at 5 min (Figure 5a–d). As the solution molarity is increased, a monotonic increase in the sulfur content is observed. When the solution molarity was increased to 0.5 mM, oxygen is completely removed from the film after 5 min. Consistent with the 0.25 mM data shown in Figure 4, under these conditions, sulfurization of the film can occur beyond the 1:1 anion exchange of oxygen with sulfur. These results demonstrate that both reaction time and solution molarity can be used as process "knobs" to tune the rate of sulfur anion exchange in Cu_2O films.

As illustrated previously in Scheme 1, as the anion-exchange process occurs, partial incorporation of sulfur into the film will be driven by diffusion from the top surface (where the film forms an interface with the solution) into the bulk of the film. Therefore, to quantitatively probe this compositional gradient through the resulting nanocomposite, XPS depth profiling was performed (Figure 6). These plots show the influence of both solution molarity and reaction time on the depth of sulfur incorporation into the films. In general, regardless of the solution molarity and reaction time, a gradient of sulfur concentration forms throughout the material thickness where sulfur concentration decreases with increasing depth. Furthermore, the extent of this sulfur incorporation is observed to increase as both the solution molarity and reaction time are increased (Figure 6a–c). We also observe that the increase in the atomic percentage of sulfur occurs more rapidly as the solution molarity is increased, compared to increasing time at a fixed concentration. These trends will be quantitatively described through a reaction-diffusion model in the anion-exchange modeling section later in this manuscript.

GIXRD Analysis. GIXRD was performed to study the impact of the Na_2S solution molarity and reaction time on the phase evolution throughout the anion-exchange process for Cu_2O

https://doi.org/10.1021/acs.chemmater.2c03773
Chem. Mater. 2023, 35, 2503–2517

films. For the lowest solution molarity (0.05 mM) (Figure S7), only minor changes in the crystallinity were observed, with only a slight reduction in the intensity of the (111) and (200) dominant Cu_2O peaks observed with increasing reaction time. As the solution molarity was increased to 0.1 and 0.25 mM (Figure S7), the reduction in Cu_2O peak intensity was more pronounced. After 20 min of anion exchange at a solution molarity of 0.25 mM, small peaks that are associated with the CuS phase began to emerge. The emergence of the crystalline CuS phase under these reaction conditions is consistent with the XPS data (Figure 4d), which showed an increase in sulfur stoichiometry beyond a 1:1 anion exchange with lattice oxygen, together with the corresponding changes in the S 2p core spectra. This provides further evidence of sulfurization of the film beyond anion-exchange chemistry, where an initial Cu_2O film can be partially converted to CuS. We further note that this phase transformation has been previously observed through high-temperature gas-phase sulfurization of Cu_2O.[56,57]

As the solution molarity was further increased to 0.5 mM (Figure 7), a significant reduction in the Cu_2O peak intensity

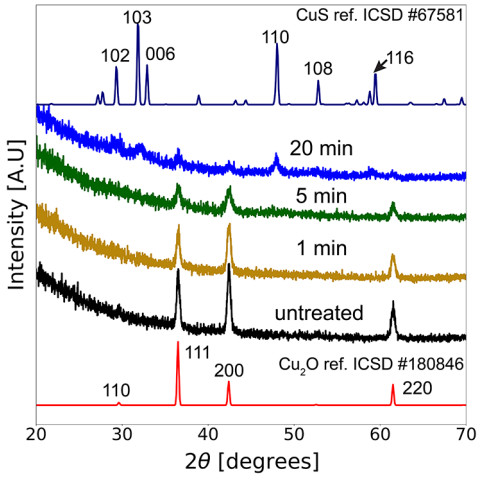

Figure 7. GIXRD patterns of sulfur-treated Cu_2O films. The anion-exchange conditions were 0.5 mM Na_2S treatment for 1, 5, and 20 min at RT.

occurs after 5 min of anion exchange. After 20 min, a two-phase mixture that is consistent with the presence of the Cu_2O and CuS phases can be clearly resolved. The presence of CuS was further evident in the corresponding synchrotron GIXRD measurements on the 20 min sample, which exhibits a clearer resolution of the CuS peaks (Figure S8).

Proposed Mechanism for Sulfur Anion Exchange and Sulfurization of Cu_2O Films. Similar to the conversion of CuO to CuS, we propose a potential mechanism for the anion exchange of Cu_2O films. When lower solution molarity and shorter reaction times are used, an amorphous copper oxysulfide layer initially forms on the film surface, as demonstrated by the lack of new crystalline peaks in the GIXRD analysis (Figure S7). This is primarily driven by anion exchange between solution sulfur species and lattice oxygen, analogous to the proposed mechanism for CuO films. For simplicity, the initial reactants S^{2-} and H_2O are left out as an alternative reaction.

$$Cu_2O + xHS^- \rightarrow Cu_2O_{(1-x)}S_x \text{ (amorphous)} + xOH^-,\ 0 \le x \le 1 \quad (3)$$

As shown by the XPS depth profiles, a sulfur concentration gradient exists throughout the material thickness, where the top surface has a higher sulfur concentration than deeper within the bulk. Hypothetically, if complete 1:1 anion exchange between lattice oxygen and solution sulfur species were to occur, the local stoichiometry could be described as

$$Cu_2O_{(1-x)}S_x \text{ (amorphous)} + (1-x)HS^- \rightarrow Cu_2S + (1-x)OH^-,\ 0 \le x \le 1 \quad (4)$$

At higher solution molarities, (i.e., 0.25 mM) and longer times (i.e., 20 min), we observe the formation of the crystalline CuS phase in both the GIXRD and XPS data, as described above. Therefore, sulfurization of the surface beyond a stoichiometry of Cu_2S may occur.

Furthermore, owing to the complexity of the copper sulfide crystal family and the challenges associated with deconvolution of these bonding environments in the XPS core spectra, it is likely that the amorphous regions of the nanocomposite likely contain a range of nonstoichiometric copper-rich sulfides and oxysulfide bonding environments (Figure 5).

AFM Analysis. The effect of solution molarity and reaction time on the surface morphology was also explored via AFM (Figure 8). Consistent with the AFM observations when CuO was the initial phase, an increase in the reaction time resulted in an increase in the surface roughness. This increase in surface roughness was observed for all solution molarities, including 0.05 mM (Figure 8a–c), 0.1 mM (Figure 8d–f), 0.25 mM (Figure 8g–i), and 0.5 mM (Figure 8j–l). As a reference, an AFM scan of a Cu_2O film prior to insertion into the anion-exchange solution is shown in Figure S9. In all instances, the anion-exchange process increases the surface roughness compared to that of the original Cu_2O film (Figure S9). We note that as the anion-exchange process continues to proceed, in some cases, the overall surface roughness may begin to decrease by filling in the gaps between surface grains since not all of the exposed facets face perpendicular to the surface normal. This creates a steric hindrance among the growing CuO_xS_y regions, where adjacent regions can obstruct the continued growth of neighboring regions, which is analogous to the morphological evolution commonly observed during hydrothermal nanowire growth.[58] Eventually, as the reaction proceeds, specific surface regions are able to grow unimpeded, which generates the larger vertical surface features observed for longer reaction times and higher solution molarities (Figure 8k,l). As discussed earlier, the ability to rationally control these changes in morphology through control of the anion-exchange process parameters provides a "knob" to tune when designing nanostructures for a specific application.

The morphological evolution of the surface topology during solution anion exchange and subsequent sulfurization of Cu_2O films is illustrated in Scheme 2. By controlling the time and/or solution molarity, hierarchical morphologies are formed, where the surface features increase in size and height as the sulfur treatment progresses. This general trend was consistent with the morphological evolution when the initial phase was CuO (Figure 3). The conformal growth of amorphous CuO_xS_y phase domains, which eventually evolve into vertical

https://doi.org/10.1021/acs.chemmater.2c03773
Chem. Mater. 2023, 35, 2503−2517

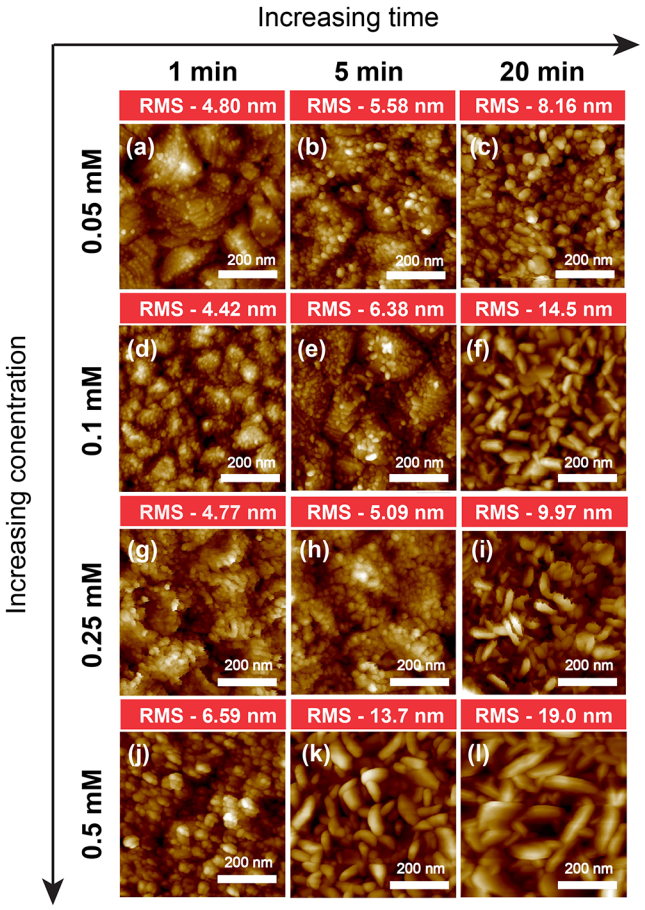

Figure 8. AFM images of Cu_2O thin films following anion exchange for 1, 5, and 20 min. Treatments were performed using solution molarities of (a–c) 0.05 mM, (d–f) 0.1 mM, (g–i) 0.25 mM, and (j–l) 0.5 mM.

Scheme 2. Illustration of Morphological Evolution during Sulfur Anion Exchange with Increasing Reaction Progress[a]

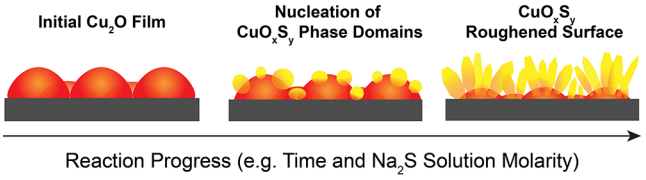

[a]In the second panel, small amorphous CuO_xS_y phase domains nucleate on the surface that eventually grow into a roughened CuO_xS_y surface. Variables that impact the reaction progress include reaction time and solution molarity.

"platelets," can be observed along the surface topology of the initial polycrystalline Cu_2O film (Figure 8).

Comparison of ALD CuO and Cu_2O Films after Anion Exchange. In the previous sections, we describe the effects of solution anion exchange on initial ALD CuO and Cu_2O films by tuning anion-exchange process variables such as the reaction time, solution molarity, and solution temperature. To provide a comparative discussion of these results, here we summarize the impact of the sulfur anion-exchange process on each initial phase.

For both the CuO and Cu_2O initial phases, XPS surface scans confirmed an inverse relationship between the intensities of the O 1s and S 2p signals as the process proceeds (Figures 1, 4, and 5), which provides evidence for successful anion exchange between oxygen and sulfur. In addition, the stoichiometry of initial Cu_2O films after sufficiently long anion-exchange times eventually surpassed a 1:1 anion-exchange condition, indicating that a sulfurization process occurs after sulfur anion exchange (Figures 4 and 5). This is further supported by GIXRD analysis, where the CuS phase is observed after 20 min at a 0.5 mM solution molarity (Figure 7). Furthermore, XPS depth profiles after anion exchange highlight the formation of sulfur gradients throughout the resulting nanocomposite thickness (Figure 6), demonstrating the diffusive nature of the anion-exchange process.

After sufficiently long reaction times and high solution molarities, both of the initial phases (CuO and Cu_2O) resulted in precipitation of the CuS phase, as demonstrated by GIXRD analysis (Figures 2 and 7). However, it was observed that the rate of conversion from CuO to CuS (Figure 2) was faster than the rate of conversion from Cu_2O to CuS (Figure 7), indicating potential differences in the diffusion and/or reaction kinetics as a function of the initial ALD phase.

Finally, the morphological changes in both initial films were evaluated by AFM. For both initial phases, we observe an increase in the RMS surface roughness after extended reaction times and increasing solution molarities. This increase in surface roughness correlates with the formation of vertical "platelets" on the top surface, which is attributed to the precipitation of the CuS phase (Figures 3 and 8). By controlling the anion-exchange reaction conditions, the surface roughness and morphologies can be tuned, enabling a range of achievable compositions and structures. In summary, we observe that the dynamic evolution of the material phase and morphology varies with respect to the initial copper oxide phase, providing a "knob" that can be tuned when designing the final material structure.

Reaction-Diffusion Model of the Anion-Exchange Process. To develop a more quantitative framework for understanding the anion-exchange process, a reaction-diffusion model was developed, which can enable predictive control of the sulfur profile throughout the converted material thickness. The anion-exchange process from Cu_2O to CuO_xS_y was modeled to describe the trends observed in the XPS compositional analysis in Figure 6. A complete list of assumptions in the model is provided in Supporting Note 2. One-dimensional (1D) Fickian diffusion can be described using eq 5

$$C(x, t) = C_{sur}\left[\mathrm{erfc}\left(\frac{x}{2(D_{eff}t)^{1/2}}\right)\right] \quad (5)$$

where C is the sulfur concentration in the material [mol/m^3], C_{sur} is the surface concentration [mol/m^3], x is position [m], t is time [s], D_{eff} is the effective diffusivity [cm^2/s], and erfc is the complementary error function.

A recent study applied Fick's second law of diffusion with a constant surface concentration of sulfur in the solid phase to model sulfur anion exchange in Fe_3O_4 nanoparticles.[59] This study assumed that ion transfer across the liquid–solid interface is fast and not rate-limiting, resulting in the initial (t = 0 min) solid phase sulfur concentration on the particle surface being equivalent to that of Fe_3S_4, the fully converted phase. Under these assumptions, the dynamics of the anion-exchange process are purely determined by solid-state

https://doi.org/10.1021/acs.chemmater.2c03773
Chem. Mater. 2023, 35, 2503–2517

diffusion. However, this assumption does not apply well to the anion-exchange system in this study, because we observe that the evolution of the sulfur depth profile varies with Na_2S solution molarity (Figure 6). If ion transfer across the liquid−solid interface was not limiting (and could thus be neglected), the surface concentration of sulfur in the material would be constant at all times regardless of the Na_2S solution molarity. However, as shown from the XPS depth profile data in Figure 6, both the surface concentration of sulfur and the concentration gradient throughout the converted material depend on the Na_2S solution molarity. This implies that the time-dependent flux of sulfur across the solid−liquid interface must be taken into account. Therefore, we introduce a reaction-diffusion model to more accurately describe the sulfur anion-exchange process.

In this study, to account for the dynamic ion-transfer rate across the interface, we incorporated first-order reaction kinetics[60] to describe the anion-exchange process across the solid-solution interface, as shown in eq 6

$$S_{sol} \underset{k_2}{\overset{k_1}{\leftrightarrow}} S_{sur} \tag{6}$$

where S_{sol} is sulfur in the solution, S_{sur} is sulfur at the film surface, and k_1 and k_2 are the rate constants of the forward and reverse reactions [m/s], respectively. The forward reaction is assumed to dominate (details in Supporting Note 2), resulting in a sulfur anion flux across the solid−liquid interface ($F_{sol\rightarrow sur}$) as described in eq 7

$$F_{sol\rightarrow sur} = hC_{sol} \tag{7}$$

where h is the interface transfer coefficient (equivalent to k_1) and C_{sol} is the sulfur concentration in solution [mol/m^3].

The change in the sulfur profile through the material thickness as a function of time can be estimated using bulk Fickian diffusion (eq 5) to solve for the sulfur concentration in the material, with first-order reaction kinetics to describe interfacial transfer (eq 7) as a boundary condition. There is assumed to be no sulfur transfer across the film-substrate (CuO_xS_y−SiO_2) interface, providing the second boundary condition. Modeling was performed numerically using a sufficiently small timestep (details in Supporting Note 2).[60] The time-dependent values for h and D_{eff} were varied and fitted to the experimental sulfur profiles for each condition (Figure 6). Trends in the fits can be seen in Figure S10.

The fitted values for D_{eff} and h were relatively consistent in samples with the same total anion-exchange time (Supporting Note 2) but varied as the anion-exchange time was increased (Table 1). Therefore, for the sake of simplicity, each fit was performed using singular values for D_{eff} and h, which represent a weighted average of the time-dependent values of these variables throughout the duration of anion exchange. These time-dependent changes in D_{eff} are expected because of the evolving phase (Figures 7 and S7) and/or morphology (Figure 8) with respect to time during anion exchange.[61] For example, as specific locations of the film are converted from Cu_2O to CuO_xS_y, the effective solid-state diffusivity of sulfur in the Cu_2O/CuO_xS_y composite will change. Morphology changes, such as the observed increase in surface roughness, could also lead to changes in D_{eff}, which are not accounted for in the 1D model in this work. Finally, although diffusion of sulfur ions was assumed to be rate-limiting, the rate-determining species may vary as film conversion proceeds and the material composition and phase changes. For example, previous studies have reported that oxygen or copper ion diffusion can also be rate-limiting in anion conversion from Cu_2O to CuS_y.[57,62−64] Therefore, while the proposed model is not intended to fully incorporate the complex and dynamic physicochemical changes occurring during anion exchange, as shown in Figure 9, the model provides a representative reduced-order description of the process.

Table 1. Fitted D_{eff} and h Values with Respect to Time Used for Anion-Exchange Modeling in Cu_2O Films

anion-exchange time (min)	1	5	20
D_{eff} (cm^2/s, $\times10^{-16}$)	37	14	8
h (cm/s, $\times10^{-4}$)	10	8	5

In addition to changes in D_{eff}, we also observe that the fitted values of h evolve as the reaction proceeds. One potential contributing factor to these changes in the fitted rate constant is the observed increases in surface roughness factor. The 1D model used here does not account for changes in the areal ionic flux across the interface associated with changes in morphology, which will affect the fitted values of h. Furthermore, as shown by the XRD data (Figures 7 and S7), a loss of crystallinity is observed as sulfur is incorporated into the oxide film, which will also influence h. In the future, multiscale computational studies that investigate the influence of evolving material composition, phase, and morphology on the values of h and D_{eff} would be useful to further understand these trends. We note that the solution molarity does not change significantly throughout the reaction since the total sulfur content in the solution was significantly larger than the sulfur content in the final converted material (Supporting Note 2).

In Figure 9, the modeled sulfur profiles using the D_{eff} and h values shown in Table 1 are compared to the experimental XPS depth profile data. Reasonably good agreement ($R^2 > 0.92$ for all conditions except for C_{sol} = 0.25 mM, t = 1 min, where R^2 = 0.82) between the modeled and experimental results is found for each condition. The 0.25 mM, 20 min case is excluded due to poor fits, likely due to the increasingly drastic changes in morphology that were observed by AFM (Figure 8) and/or more pronounced changes in crystallinity (Figures 7 and S7).

Despite the aforementioned simplifications and assumptions, the model developed in this work enables the prediction and rational control of sulfur anion exchange under specified conditions, especially when large changes in the surface morphology and phase are absent. In the future, a 2D or 3D model could be developed to help account for morphology changes, and multicomponent diffusion could be incorporated to describe conversion of films during significant changes in composition and phase.

Sulfur Anion Exchange on a High-Aspect-Ratio Structure. As discussed earlier, one of the major advantages of ALD compared to alternative thin-film deposition processes is the ability to conformally coat high-aspect-ratio structures, without line-of-sight limitations.[65] Therefore, to evaluate the ability of the anion-exchange process to maintain the conformal and uniform coating geometry of the original ALD film, we deposited an ∼30 nm CuO coating onto the surface of a ZnO nanowire (NW) array grown by hydrothermal synthesis. An SEM image of the ZnO nanowire array is shown in Figure S11. To protect the underlying ZnO NW core from reaction with the anion-exchange solution, a 5 nm TiO_2

https://doi.org/10.1021/acs.chemmater.2c03773
Chem. Mater. 2023, 35, 2503−2517

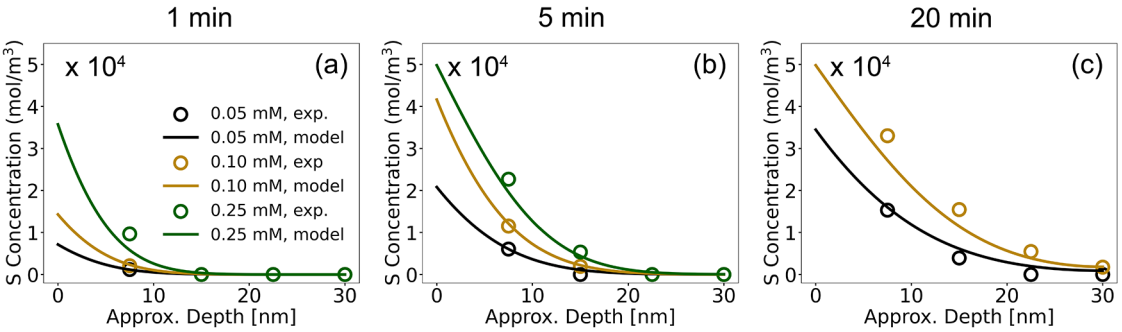

Figure 9. Modeled and experimental XPS depth profile data of sulfur concentration for times of (a) 1 min, (b) 5 min, and (c) 20 min when the initial phase was Cu_2O.

diffusion barrier layer was deposited using ALD between the ZnO and CuO, forming a core−shell−shell NW. ZnO has a narrow pH stability window and is also known to react with Na_2S solutions, whereas ALD TiO_2 is stable under the solution reaction conditions used in this study (further details in Figure S12).[66] Details of the hydrothermal synthesis method[46] and the TiO_2 barrier layer deposition conditions can be found in Supporting Note 1.

After anion exchange in a 0.5 mM solution for 1 min at 80 °C, a conformal layer of CuO_xS_y was visible, which can be seen in the HAADF-STEM (Figure 10a) and EELS elemental maps

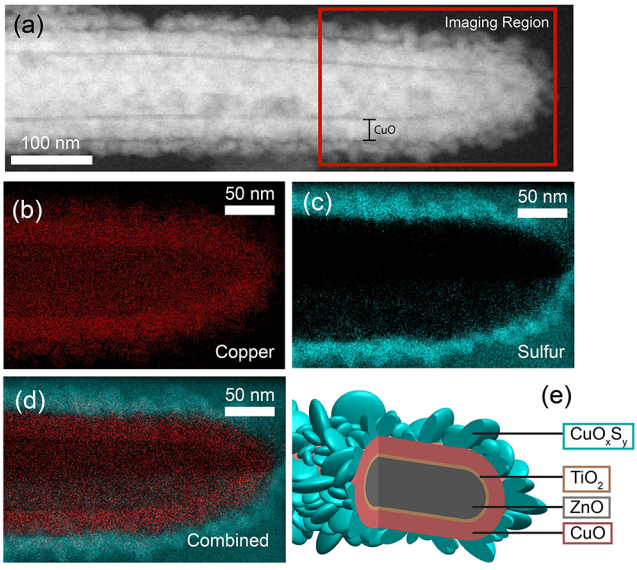

Figure 10. (a) HAADF-STEM of ZnO nanowire/5 nm TiO_2/~30 nm CuO layer after anion exchange in a 0.5 mM Na_2S solution for 1 min at 80 °C. (b, c) EELS elemental maps of elemental Cu and S. (d) Combined EELS map with Cu and S overlay (e) Schematic representation of the ZnO NW/5 nm TiO_2/~30 nm CuO after anion exchange.

(Figure 10b−d). A schematic representation of the core−shell−shell nanowire after anion exchange is presented in Figure 10e. This morphology is analogous to that which was observed in the planar samples, where sulfur diffuses into the initial CuO film, generating a compositional gradient that is sulfur-rich on the outer surface while preserving the underlying CuO film. This provides a proof-of-concept demonstration that solution sulfur anion exchange can be integrated with ALD to form conformal sulfur-containing compounds on high-aspect-ratio structures.

Area-Selective Anion Exchange on Patterned CuO_x Samples. As described in the preceding sections, the solution anion exchange of ALD films allows for facile conversion of the chemical, structural, and morphological properties of the resulting surfaces with tunable control. The relatively mild temperatures and pH values of this aqueous solution process can be further integrated with standard patterning processes such as photolithography. In particular, there is a strong interest in area-selective deposition processes, where selective reactions occur in patterned regions of the substrate.[67,68] Therefore, to demonstrate the ability to selectively pattern ALD film surfaces using this approach, anion exchange was performed on substrates patterned with photoresist.

Figure 11 shows the results of area-selective anion exchange on both Cu_2O (Figure 11a−d) and CuO (Figure 11e−h) initial films. Rectangular regions were lithographically patterned to expose the underlying ALD CuO_x film, which were subsequently inserted into a 0.5 mM Na_2S solution for 1 min. For the Cu_2O film, following photoresist removal, a clear contrast in the SEM images was observed between the sulfur-treated and untreated Cu_2O regions (Figure 11a). Sulfur EDS line scans demonstrate the presence of sulfur only in the regions where anion exchange occurs (Figure 11b). Additionally, an inverse relationship is observed between the oxygen and sulfur signals, where sulfur increases in the regions where oxygen decreases. Using this technique, we are able to successfully resolve a microscale untreated region of the original Cu_2O film (Figure 11b), demonstrating the ability to use area-selective anion exchange for micro-patterning of functional materials.

Area-selective anion exchange was also demonstrated for an initial CuO film. Similar trends are observed in the SEM and EDS line scan data (Figure 11e,f). The regions of the sample that were exposed to the Na_2S solution exhibit a nonzero sulfur signal and low oxygen signal, whereas the inverse trend is observed in the regions that were covered with photoresist, where no sulfur was observed, and the oxygen signal increases (Figure 11f). Additional EDS point scans were collected in these two distinct regions, further confirming the absence of sulfur in the patterned area (Figure S13).

Finally, a ring-patterned region with an elemental sulfur map further illustrates the area-selective sulfur anion exchange of both the Cu_2O (Figure 11c,d) and CuO films (Figure 11g,h) after sulfur treatment. In the future, the compatibility of ALD and sulfur anion exchange with lithographic patterning could enable novel strategies for device fabrication, such as the

https://doi.org/10.1021/acs.chemmater.2c03773
Chem. Mater. 2023, 35, 2503−2517

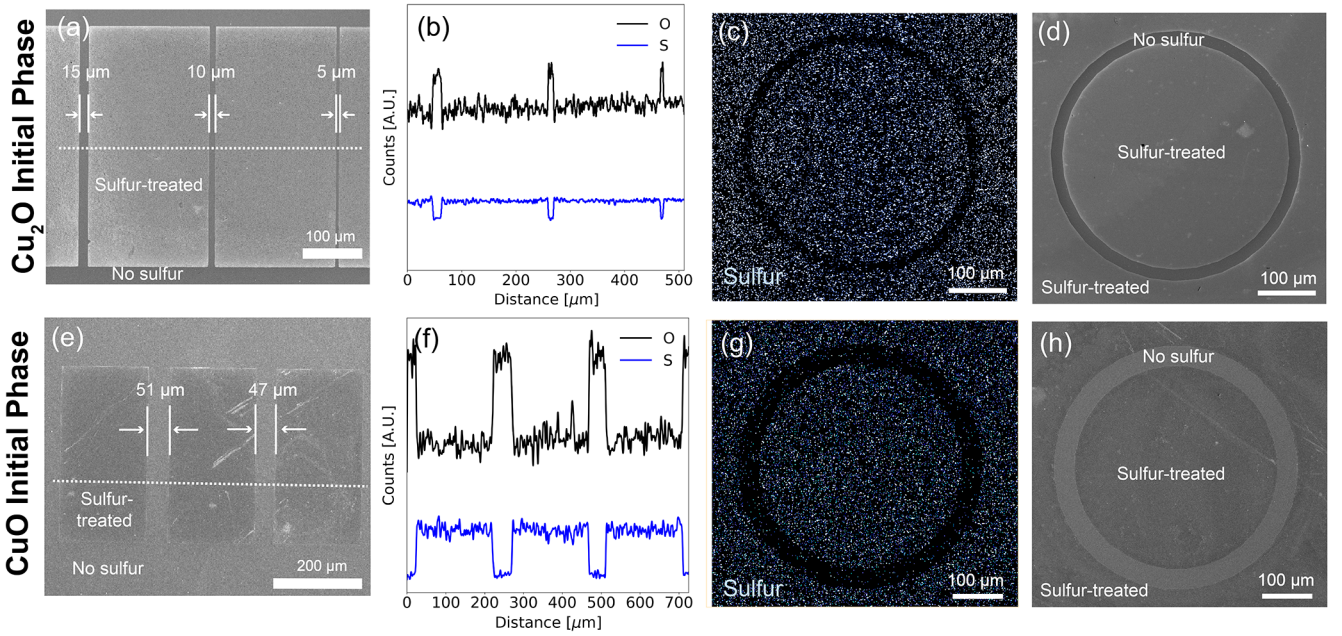

Figure 11. (a) SEM image of an initial Cu_2O film after 1 min of sulfur treatment at RT and 0.5 mM Na_2S solution molarity. The dotted line indicates the location where the EDS line scan was taken. (b) EDS line scan of O and S for the sample shown in (a). (c) Elemental sulfur map and (d) the corresponding SEM of a patterned surface from the sample shown in (a). (e) SEM image of an initial CuO film after 1 min of sulfur treatment at 80 °C and 0.5 mM Na_2S solution molarity. (f) EDS line scan of O and S for the sample shown in (e). (g) Elemental sulfur map and (h) the corresponding SEM of a patterned surface from the sample shown in (e).

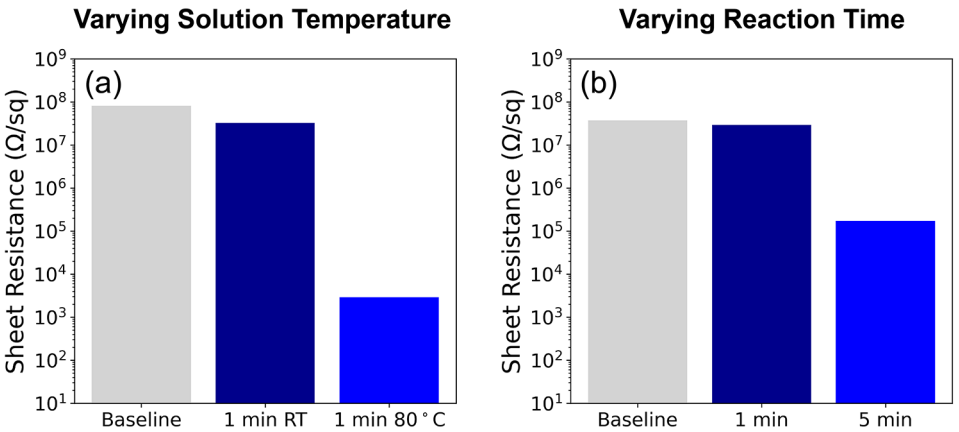

Figure 12. Trends in the electrical sheet resistance of the films after different sulfur treatment conditions. (a) Variations in solution temperature (RT vs 80 °C) using 0.5 mM Na_2S solution molarity for 1 min with an initial phase of CuO. (b) Varying sulfur treatment time using 0.05 mM Na_2S at RT with an initial phase of Cu_2O. The baseline film represents the electrical sheet resistance of the initial CuO or Cu_2O films before anion exchange. Note the logarithmic scale.

formation of copper oxide/copper sulfide semiconductor heterojunctions or doping of the surface to minimize contact resistance. Therefore, in the following section, we examine the impact of sulfur anion exchange on the electrical properties of the material.

Electrical Characterization. To determine the effect of the anion-exchange conditions (i.e., sulfur content) on the electrical properties of semiconductor devices, electrical sheet resistance measurements were performed. By controlling the reaction time, temperature, and solution molarity, large effects were observed on the electronic properties of the resulting nanocomposite. The family of copper sulfides (e.g., CuS and Cu_2S) are typically p-type semiconductors with high carrier concentrations, which originate from the presence of a large number of native Cu vacancies.[69,70] For instance, CuS is a p-type semiconductor with a bandgap in the range of ∼2.4 to 2.5 eV,[13] which typically exhibits low electrical resistivities on the order of $\sim 10^{-4}$ Ω cm.[71]

When the reaction temperature of an initial CuO film was varied from RT to 80 °C, (Figure 12a) at a constant reaction time of 1 min and solution molarity of 0.5 mM Na_2S, a decrease in the sheet resistance was observed, compared to the baseline value of 8.1×10^7 Ω/sq in the untreated film. Following anion exchange at RT, the sheet resistance was only slightly reduced to 3.3×10^7 Ω/sq, while treatment at 80 °C resulted in a decrease in sheet resistance of greater than 4 orders of magnitude to 2860 Ω/sq. This is consistent with our

https://doi.org/10.1021/acs.chemmater.2c03773
Chem. Mater. 2023, 35, 2503−2517

experimental observations that anion exchange proceeds more rapidly at an elevated temperature.

The sheet resistances after anion exchange when the initial phase was Cu_2O were also investigated. Figure 12b shows the influence of reaction time on sheet resistance using a low solution molarity of 0.05 mM at RT. We observe that after 1 min, the sheet resistance decreases by 22%, whereas after 5 min, the sheet resistance has decreased by more than 2 orders of magnitude. While the GIXRD analysis under these conditions demonstrates that the phase remains as Cu_2O (Figure S7), XPS analysis shows an increase in the surface sulfur content from ∼1 to ∼5% (Figure 6). This demonstrates that mild incorporation of sulfur at doping concentrations can significantly impact the electronic properties of the original Cu_2O film.

The ability to adjust the sheet resistance through anion exchange could potentially be exploited to modify surfaces and interfaces where lower sheet resistance is required. For example, in thin-film transistors, creating a heavily doped semiconductor region under the source/drain contacts can reduce deleteriously high contact resistances typically found for wide bandgap p-type oxides.[72] Furthermore, the ability to rationally control the depth of anion exchange, which we demonstrate through the modeling and experimental results above, can be used to decouple the electrical properties of the surface from those of the underlying bulk material.

CONCLUSIONS

In this study, sulfur anion-exchange reactions were performed on ALD CuO and Cu_2O films, demonstrating an approach to deposit metal sulfide or oxysulfide layers without the use of H_2S gas. By systematically changing the solution molarity, time, and temperature, the film stoichiometry and phases present can be tuned, enabling versatile accessible chemical compositions. In the early stages of anion exchange, a decrease in the initial CuO_x film crystallinity was observed as sulfur was increasingly incorporated into the film. After extended anion exchange, the formation of a crystalline CuS phase was observed. For the films that were initially Cu_2O, the formation of CuS indicates that sulfurization continues to occur even after the sulfur-oxygen exchange was complete. The extent of these changes in the crystal phase was observed to increase with higher reaction temperatures, larger Na_2S solution molarity, and longer reaction times.

The surface roughness and morphology of the initial CuO_x films were also highly correlated with increasing anion exchange, which eventually forms a hierarchal morphology consisting of surface platelets that nucleate and grow on top of the underlying CuO_x grains. The relationship between the surface roughness and morphology can be utilized to develop high-surface-area catalysts or minimized for electrical devices.

XPS depth profiles demonstrate a gradient in sulfur content from the surface into the bulk of the material after anion exchange. To describe this compositional evolution, a reaction-diffusion model was developed which enables predictive control of the anion conversion process with respect to Na_2S solution molarity and reaction time. Overall, this detailed process-structure knowledge provides a foundation to tune the composition, phase, and morphology of ALD films, opening up new possibilities to expand the ALD synthesis "toolbox."

Electrical sheet resistance measurements after sulfur anion exchange chemistry demonstrate a tunable reduction of the sheet resistance by up to 4 orders of magnitude as the sulfur content in the material increases. This demonstrates a pathway for doping and/or conversion into new semiconducting phases, which could be utilized to reduce bulk or interfacial resistance in electronic devices. In addition, sulfur anion exchange was performed on a $ZnO@TiO_2@CuO$ core−shell−shell nanowire, illustrating that the anion-exchange process maintains the conformality of the initial ALD process. In the future, the anion-exchange process can be performed on other 3D substrates and high-aspect-ratio structures. To demonstrate a pathway toward applying sulfur anion exchange of ALD films toward device applications, CuO_x films were lithographically patterned to perform area-selective anion exchange. The compatibility of the sequential ALD and anion-exchange process with lithographic patterning shows promise for integration with the microfabrication of layered devices. In the future, we anticipate that this approach can be used to tune sulfur incorporation into ALD films for a broad range of applications where concurrent and tunable control of material composition, phase, and morphology are critical, including catalysis, photovoltaic and electronic devices.

ASSOCIATED CONTENT

Supporting Information

The Supporting Information is available free of charge at https://pubs.acs.org/doi/10.1021/acs.chemmater.2c03773.

Further experimental details on nanowire preparation, additional XPS survey scans and core scans, synchrotron GIXRD data, AFM images before anion exchange, additional benchtop GIXRD data, supplementary modeling details and assumptions, SEM of a nanowire array, and EDS spectra after area-selective sulfur anion exchange (PDF)

AUTHOR INFORMATION

Corresponding Author

Neil P. Dasgupta − *Department of Materials Science and Engineering, University of Michigan, Ann Arbor, Michigan 48109, United States; Department of Mechanical Engineering, University of Michigan, Ann Arbor, Michigan 48109, United States;* orcid.org/0000-0002-5180-4063; Email: ndasgupt@umich.edu

Authors

Julia D. Lenef − *Department of Materials Science and Engineering, University of Michigan, Ann Arbor, Michigan 48109, United States*

Andrew J. Gayle − *Department of Mechanical Engineering, University of Michigan, Ann Arbor, Michigan 48109, United States*

Jaesung Jo − *Department of Electrical Engineering and Computer Science, University of Michigan, Ann Arbor, Michigan 48109, United States*

Kalyn M. Fuelling − *Department of Materials Science and Engineering, University of Michigan, Ann Arbor, Michigan 48109, United States*

Srinivas K. Yadavalli − *Department of Mechanical Engineering, University of Michigan, Ann Arbor, Michigan 48109, United States*

Alondra M. Ortiz-Ortiz − *Department of Mechanical Engineering, University of Michigan, Ann Arbor, Michigan 48109, United States*

Kai Sun − *Department of Materials Science and Engineering, University of Michigan, Ann Arbor, Michigan 48109, United States;* orcid.org/0000-0003-1745-9136

Rebecca L. Peterson − *Department of Materials Science and Engineering, University of Michigan, Ann Arbor, Michigan 48109, United States; Department of Electrical Engineering and Computer Science, University of Michigan, Ann Arbor, Michigan 48109, United States;* orcid.org/0000-0001-9405-6539

Complete contact information is available at: https://pubs.acs.org/10.1021/acs.chemmater.2c03773

Author Contributions

The manuscript was written through contributions of all authors. All authors have given approval to the final version of the manuscript.

Notes

The authors declare no competing financial interest.

■ ACKNOWLEDGMENTS

This research was supported by Intel Corporation through an Intel Strategic Research Alliance (ISRA). The authors thank Intel Components Research for engaging in discussion and financial support. This material is based upon work supported by the National Science Foundation under grant nos. 1727918 and 1751590. A.J.G. and A.M.O.-O. acknowledge support from the National Science Foundation Graduate Research Fellowship Program under Grant No. DGE-1256260. The authors also thank Tae H. Cho for deposition of the TiO_2 interlayer and Adrian J. Sanchez for assistance with signal processing. Portions of this work were performed in the Michigan Center for Materials Characterization and the Lurie Nanofabrication Facility, which are supported by the University of Michigan's College of Engineering. The authors acknowledge staff scientists Bobby Kerns for assistance on SEM and Haiping Sun for AFM guidance. Synchrotron GIXRD measurements were taken at the Advanced Photon Source, a U.S. Department of Energy (DOE) facility using beamline 33-BM-C at Argonne National Laboratory. The authors thank beamline scientist Evguenia Karapetrova for her assistance and training.

■ REFERENCES

(1) Foley, S.; Geaney, H.; Bree, G.; Stokes, K.; Connolly, S.; Zaworotko, M. J.; Ryan, K. M. Copper Sulfide (Cu_xS) Nanowire-in-Carbon Composites Formed from Direct Sulfurization of the Metal-Organic Framework HKUST-1 and Their Use as Li-Ion Battery Cathodes. *Adv. Funct. Mater.* **2018**, *28*, No. 1800587.

(2) Meng, X.; He, K.; Su, D.; Zhang, X.; Sun, C.; Ren, Y.; Wang, H.-H.; Weng, W.; Trahey, L.; Canlas, C. P.; Elam, J. W. Gallium Sulfide−Single-Walled Carbon Nanotube Composites: High-Performance Anodes for Lithium-Ion Batteries. *Adv. Funct. Mater.* **2014**, *24*, 5435−5442.

(3) Dubale, A. A.; Tamirat, A. G.; Chen, H.-M.; Berhe, T. A.; Pan, C.-J.; Su, W.-N.; Hwang, B.-J. A Highly Stable CuS and CuS−Pt Modified Cu_2O/CuO Heterostructure as an Efficient Photocathode for the Hydrogen Evolution Reaction. *J. Mater. Chem. A* **2016**, *4*, 2205−2216.

(4) He, J.; Chen, Y.; Manthiram, A. Metal Sulfide-Decorated Carbon Sponge as a Highly Efficient Electrocatalyst and Absorbant for Polysulfide in High-Loading Li_2S Batteries. *Adv. Energy Mater.* **2019**, *9*, No. 1900584.

(5) van Oversteeg, C. H. M.; Tapia Rosales, M.; Helfferich, K. H.; Ghiasi, M.; Meeldijk, J. D.; Firet, N. J.; Ngene, P.; de Mello Donegá, C.; de Jongh, P. E. Copper Sulfide Derived Nanoparticles Supported on Carbon for the Electrochemical Reduction of Carbon Dioxide. *Catal. Today* **2021**, *377*, 157−165.

(6) Yang, D.; Cho, I.; Kim, D.; Lim, M. A.; Li, Z.; Ok, J. G.; Lee, M.; Park, I. Gas Sensor by Direct Growth and Functionalization of Metal Oxide/Metal Sulfide Core−Shell Nanowires on Flexible Substrates. *ACS Appl. Mater. Interfaces* **2019**, *11*, 24298−24307.

(7) Sam, M.; Bayati, M. R.; Mojtahedi, M.; Janghorban, K. Growth of Cu2S/CdS Nano-Layered Photovoltaic Junctions for Solar Cell Applications. *Appl. Surf. Sci.* **2010**, *257*, 1449−1453.

(8) Mude, N. N.; Bukke, R. N.; Jang, J. High Performance of Solution-Processed Amorphous p-Channel Copper-Tin-Sulfur-Gallium Oxide Thin-Film Transistors by UV/O_3 Photocuring. *ACS Appl. Mater. Interfaces* **2021**, *13*, 20277−20287.

(9) George, S. M. Atomic Layer Deposition: An Overview. *Chem. Rev.* **2010**, *110*, 111−131.

(10) Dasgupta, N. P.; Lee, H.-B.-R.; Bent, S. F.; Weiss, P. S. Recent Advances in Atomic Layer Deposition. *Chem. Mater.* **2016**, *28*, 1943−1947.

(11) Dasgupta, N. P.; Meng, X.; Elam, J. W.; Martinson, A. B. F. Atomic Layer Deposition of Metal Sulfide Materials. *Acc. Chem. Res.* **2015**, *48*, 341−348.

(12) Dasgupta, N. P.; Mack, J. F.; Langston, M. C.; Bousetta, A.; Prinz, F. B. Design of an Atomic Layer Deposition Reactor for Hydrogen Sulfide Compatibility. *Rev. Sci. Instrum.* **2010**, *81*, No. 044102.

(13) Tripathi, T. S.; Lahtinen, J.; Karppinen, M. Atomic Layer Deposition of Conducting CuS Thin Films from Elemental Sulfur. *Adv. Mater. Interfaces* **2018**, *5*, No. 1701366.

(14) Li, H.; Zhao, R.; Zhu, J.; Guo, Z.; Xiong, W.; Wang, X. Organosulfur Precursor for Atomic Layer Deposition of High-Quality Metal Sulfide Films. *Chem. Mater.* **2020**, *32*, 8885−8894.

(15) Ko, D.-H.; Kim, S.; Jin, Z.; Shin, S.; Lee, S. Y.; Min, Y.-S. A Novel Chemical Route to Atomic Layer Deposition of ZnS Thin Film from Diethylzinc and 1,5-Pentanedithiol. *Bull. Korean Chem. Soc.* **2017**, *38*, 696−699.

(16) Liu, H. F.; Antwi, K. K. A.; Wang, Y. D.; Ong, L. T.; Chua, S. J.; Chi, D. Z. Atomic Layer Deposition of Crystalline Bi_2O_3 Thin Films and Their Conversion into Bi_2S_3 by Thermal Vapor Sulfurization. *RSC Adv.* **2014**, *4*, 58724−58731.

(17) Kozodaev, M. G.; Slavich, A. S.; Romanov, R. I.; Zarubin, S. S.; Markeev, A. M. Influence of Reducing Agent on Properties of Thin WS_2 Nanosheets Prepared by Sulfurization of Atomic Layer-Deposited WO_3. *J. Phys. Chem. C* **2020**, *124*, 28169−28177.

(18) Romanov, R. I.; Kozodaev, M. G.; Myakota, D. I.; Chernikova, A. G.; Novikov, S. M.; Volkov, V. S.; Slavich, A. S.; Zarubin, S. S.; Chizhov, P. S.; Khakimov, R. R.; Chouprik, A. A.; Hwang, C. S.; Markeev, A. M. Synthesis of Large Area Two-Dimensional MoS_2 Films by Sulfurization of Atomic Layer Deposited MoO_3 Thin Film for Nanoelectronic Applications. *ACS Appl. Nano Mater.* **2019**, *2*, 7521−7531.

(19) Seenivasan, S.; Jung, H.; Han, J. W.; Kim, D.-H. Surface Roughening Strategy for Highly Efficient Bifunctional Electrocatalyst: Combination of Atomic Layer Deposition and Anion Exchange Reaction. *Small Methods* **2022**, *6*, No. 2101308.

(20) Li, N.; Feng, L.; Su, J.; Zeng, W.; Liu, Z. Optical and Electrical Properties of Al:WS_2 Films Prepared by Atomic Layer Deposition and Vulcanization. *RSC Adv.* **2016**, *6*, 64879−64884.

(21) Thimsen, E.; Peng, Q.; Martinson, A. B. F.; Pellin, M. J.; Elam, J. W. Ion Exchange in Ultrathin Films of Cu_2S and ZnS under Atomic Layer Deposition Conditions. *Chem. Mater.* **2011**, *23*, 4411−4413.

(22) Zhu, C.; Yang, P.; Chao, D.; Wang, X.; Zhang, X.; Chen, S.; Tay, B. K.; Huang, H.; Zhang, H.; Mai, W.; Fan, H. J. All Metal Nitrides Solid-State Asymmetric Supercapacitors. *Adv. Mater.* **2015**, *27*, 4566−4571.

(23) Luo, J.; Karuturi, S. K.; Liu, L.; Su, L. T.; Tok, A. I. Y.; Fan, H. J. Homogeneous Photosensitization of Complex TiO_2 Nanostructures for Efficient Solar Energy Conversion. *Sci. Rep.* **2012**, *2*, No. 451.

(24) Lee, Y.-I. Selective Transformation of Cu Nanowires to Cu_2S or CuS Nanostructures and the Roles of the Kirkendall Effect and Anion Exchange Reaction. *Mater. Chem. Phys.* **2016**, *180*, 104−113.
(25) Ma, R.; Levard, C.; Michel, F. M.; Brown, G. E.; Lowry, G. V. Sulfidation Mechanism for Zinc Oxide Nanoparticles and the Effect of Sulfidation on Their Solubility. *Environ. Sci. Technol.* **2013**, *47*, 2527−2534.
(26) Xia, X.; Zhu, C.; Luo, J.; Zeng, Z.; Guan, C.; Ng, C. F.; Zhang, H.; Fan, H. J. Synthesis of Free-Standing Metal Sulfide Nanoarrays via Anion Exchange Reaction and Their Electrochemical Energy Storage Application. *Small* **2014**, *10*, 766−773.
(27) Brittman, S.; Yoo, Y.; Dasgupta, N. P.; Kim, S.; Kim, B.; Yang, P. Epitaxially Aligned Cuprous Oxide Nanowires for All-Oxide, Single-Wire Solar Cells. *Nano Lett.* **2014**, *14*, 4665−4670.
(28) Yuan, K. D.; Wu, J. J.; Liu, M. L.; Zhang, L. L.; Xu, F. F.; Chen, L. D.; Huang, F. Q. Fabrication and Microstructure of p-Type Transparent Conducting CuS Thin Film and Its Application in Dye-Sensitized Solar Cell. *Appl. Phys. Lett.* **2008**, *93*, No. 132106.
(29) Hall, R. B.; Meakin, J. D. The Design and Fabrication of High Efficiency Thin Film CdS/Cu_2S Solar Cells. *Thin Solid Films* **1979**, *63*, 203−211.
(30) Al-Jawhari, H. A. A Review of Recent Advances in Transparent p-Type Cu_2O-Based Thin Film Transistors. *Mater. Sci. Semicond. Process.* **2015**, *40*, 241−252.
(31) Sanal, K. C.; Vikas, L. S.; Jayaraj, M. K. Room Temperature Deposited Transparent P-Channel CuO Thin Film Transistors. *Appl. Surf. Sci.* **2014**, *297*, 153−157.
(32) de Carvalho, C. N.; Parreira, P.; Lavareda, G.; Brogueira, P.; Amaral, A. p-Type Cu_xS Thin Films: Integration in a Thin Film Transistor Structure. *Thin Solid Films* **2013**, *543*, 3−6.
(33) Cheng, D.; Zhao, Z.-J.; Zhang, G.; Yang, P.; Li, L.; Gao, H.; Liu, S.; Chang, X.; Chen, S.; Wang, T.; Ozin, G. A.; Liu, Z.; Gong, J. The Nature of Active Sites for Carbon Dioxide Electroreduction over Oxide-Derived Copper Catalysts. *Nat. Commun.* **2021**, *12*, No. 395.
(34) Kim, Y.; Park, K. Y.; Jang, D. M.; Song, Y. M.; Kim, H. S.; Cho, Y. J.; Myung, Y.; Park, J. Synthesis of Au−Cu_2S Core−Shell Nanocrystals and Their Photocatalytic and Electrocatalytic Activity. *J. Phys. Chem. C* **2010**, *114*, 22141−22146.
(35) Meyer, B. K.; Merita, S.; Polity, A. On the Synthesis and Properties of Ternary Copper Oxide Sulfides ($Cu_2O_{1-x}S_x$). *Phys. Status Solidi RRL* **2013**, *7*, 360−363.
(36) Wei, C.; Zou, X.; Liu, Q.; Li, S.; Kang, C.; Xiang, W. A Highly Sensitive Non-Enzymatic Glucose Sensor Based on CuS Nanosheets Modified Cu_2O/CuO Nanowire Arrays. *Electrochim. Acta* **2020**, *334*, No. 135630.
(37) Panzeri, G.; Cristina, M.; Jagadeesh, M. S.; Bussetti, G.; Magagnin, L. Modification of Large Area Cu_2O/CuO Photocathode with CuS Non-Noble Catalyst for Improved Photocurrent and Stability. *Sci. Rep.* **2020**, *10*, No. 18730.
(38) Gunasekaran, S.; Thangaraju, D.; Marnadu, R.; Chandrasekaran, J.; Shkir, M.; Durairajan, A.; Valente, M. A.; Alshaharani, T.; Elango, M. Photosensitive Activity of Fabricated Core-Shell Composite Nanostructured p-CuO@CuS/n-Si Diode for Photodetection Applications. *Sens. Actuators, A* **2021**, *317*, No. 112373.
(39) Huang, Y.; Deng, Y.; Handoko, A. D.; Goh, G. K. L.; Yeo, B. S. Rational Design of Sulfur-Doped Copper Catalysts for the Selective Electroreduction of Carbon Dioxide to Formate. *ChemSusChem* **2018**, *11*, 320−326.
(40) Zhang, X.; Cui, X.; Sun, Y.; Qi, K.; Jin, Z.; Wei, S.; Li, W.; Zhang, L.; Zheng, W. Nanoporous Sulfur-Doped Copper Oxide ($Cu_2O_xS_{1-x}$) for Overall Water Splitting. *ACS Appl. Mater. Interfaces* **2018**, *10*, 745−752.
(41) Stevanović, V.; Zakutayev, A.; Lany, S. Composition Dependence of the Band Gap and Doping in Cu_2O-Based Alloys as Predicted by an Extension of the Dilute-Defect Model. *Phys. Rev. Appl.* **2014**, *2*, No. 044005.
(42) Ma, R.; Stegemeier, J.; Levard, C.; G Dale, J.; W Noack, C.; Yang, T.; E Brown, G.; V Lowry, G. Sulfidation of Copper Oxide Nanoparticles and Properties of Resulting Copper Sulfide. *Environ. Sci.: Nano* **2014**, *1*, 347−357.
(43) Xiong, S.; Zeng, H. C. Serial Ionic Exchange for the Synthesis of Multishelled Copper Sulfide Hollow Spheres. *Angew. Chem.* **2012**, *124*, 973−976.
(44) Zhang, D.-F.; Zhang, H.; Shang, Y.; Guo, L. Stoichiometry-Controlled Fabrication of Cu_xS Hollow Structures with Cu_2O as Sacrificial Templates. *Cryst. Growth Des.* **2011**, *11*, 3748−3753.
(45) Lenef, J. D.; Jo, J.; Trejo, O.; Mandia, D. J.; Peterson, R. L.; Dasgupta, N. P. Plasma-Enhanced Atomic Layer Deposition of p-Type Copper Oxide Semiconductors with Tunable Phase, Oxidation State, and Morphology. *J. Phys. Chem. C* **2021**, *125*, 9383−9390.
(46) Bielinski, A. R.; Boban, M.; He, Y.; Kazyak, E.; Lee, D. H.; Wang, C.; Tuteja, A.; Dasgupta, N. P. Rational Design of Hyperbranched Nanowire Systems for Tunable Superomniphobic Surfaces Enabled by Atomic Layer Deposition. *ACS Nano* **2017**, *11*, 478−489.
(47) Kundu, M.; Hasegawa, T.; Terabe, K.; Yamamoto, K.; Aono, M. Structural Studies of Copper Sulfide Films: Effect of Ambient Atmosphere. *Sci. Technol. Adv. Mater.* **2008**, *9*, No. 035011.
(48) Xie, Y.; Riedinger, A.; Prato, M.; Casu, A.; Genovese, A.; Guardia, P.; Sottini, S.; Sangregorio, C.; Miszta, K.; Ghosh, S.; Pellegrino, T.; Manna, L. Copper Sulfide Nanocrystals with Tunable Composition by Reduction of Covellite Nanocrystals with Cu^+ Ions. *J. Am. Chem. Soc.* **2013**, *135*, 17630−17637.
(49) Biesinger, M. C. Advanced Analysis of Copper X-Ray Photoelectron Spectra: Advanced Analysis of Copper X-Ray Photoelectron Spectra. *Surf. Interface Anal.* **2017**, *49*, 1325−1334.
(50) Payne, B. P.; Biesinger, M. C.; McIntyre, N. S. The Study of Polycrystalline Nickel Metal Oxidation by Water Vapour. *J. Electron Spectrosc. Relat. Phenom.* **2009**, *175*, 55−65.
(51) Chawla, S. K.; Sankarraman, N.; Payer, J. H. Diagnostic spectra for XPS analysis of Cu-O-S-H compounds. *J. Electron Spectrosc. Relat. Phenom.* **1992**, *61*, 1−18.
(52) Minguez-Bacho, I.; Courté, M.; Fan, H. J.; Fichou, D. Conformal Cu_2S-Coated Cu_2O Nanostructures Grown by Ion Exchange Reaction and Their Photoelectrochemical Properties. *Nanotechnology* **2015**, *26*, No. 185401.
(53) Kung, C.-W.; Chen, H.-W.; Lin, C.-Y.; Huang, K.-C.; Vittal, R.; Ho, K.-C. CoS Acicular Nanorod Arrays for the Counter Electrode of an Efficient Dye-Sensitized Solar Cell. *ACS Nano* **2012**, *6*, 7016−7025.
(54) Hu, X.-S.; Shen, Y.; Xu, L.-H.; Wang, L.; Lu, L.-S.; Zhang, Y.-T. Preparation of Flower-like CuS by Solvothermal Method for Photocatalytic, UV Protection and EMI Shielding Applications. *Appl. Surf. Sci.* **2016**, *385*, 162−170.
(55) Barqi, J.; Masoudpanah, S. M.; Sh Bafghi, M. Facile Synthesis of Plate-Like Copper Sulfide Powder as an Electrode Material for High-Performance Supercapacitors. *J. Mater. Sci.: Mater. Electron.* **2020**, *31*, 17614−17623.
(56) Cai, L.; Sun, Y.; Li, W.; Zhang, W.; Liu, X.; Ding, D.; Xu, N. CuS Hierarchical Hollow Microcubes with Improved Visible-Light Photocatalytic Performance. *RSC Adv.* **2015**, *5*, 98136−98143.
(57) Zhu, H.; Wang, J.; Wu, D. Fast Synthesis, Formation Mechanism, and Control of Shell Thickness of CuS Hollow Spheres. *Inorg. Chem.* **2009**, *48*, 7099−7104.
(58) Bielinski, A. R.; Kazyak, E.; Schlepütz, C. M.; Jung, H. J.; Wood, K. N.; Dasgupta, N. P. Hierarchical ZnO Nanowire Growth with Tunable Orientations on Versatile Substrates Using Atomic Layer Deposition Seeding. *Chem. Mater.* **2015**, *27*, 4799−4807.
(59) Lim, Y.; Lee, C.-H.; Jun, C.-H.; Kim, K.; Cheon, J. Morphology-Conserving Non-Kirkendall Anion Exchange of Metal Oxide Nanocrystals. *J. Am. Chem. Soc.* **2020**, *142*, 9130−9134.
(60) Plummer, J. D.; Deal, M. D.; Griffin, P. B. *Silicon VLSI Technology: Fundamentals, Practice and Modeling*; Prentice Hall, 2000.
(61) Lide, D. R. *CRC Handbook of Chemistry and Physics*, 85th ed.; CRC Press, 2004.

https://doi.org/10.1021/acs.chemmater.2c03773
Chem. Mater. 2023, 35, 2503−2517

(62) Yang, Z.-h.; Zhang, D.; Zhang, W.; Chen, M. Controlled Synthesis of Cuprous Oxide Nanospheres and Copper Sulfide Hollow Nanospheres. *J. Phys. Chem. Solids* **2009**, *70*, 840−846.
(63) Cao, H.; Qian, X.; Wang, C.; Ma, X.; Yin, J.; Zhu, Z. High Symmetric 18-Facet Polyhedron Nanocrystals of Cu_7S_4 with a Hollow Nanocage. *J. Am. Chem. Soc.* **2005**, *127*, 16024−16025.
(64) Jiao, S.; Xu, L.; Jiang, K.; Xu, D. Well-Defined Non-Spherical Copper Sulfide Mesocages with Single-Crystalline Shells by Shape-Controlled Cu_2O Crystal Templating. *Adv. Mater.* **2006**, *18*, 1174−1177.
(65) Gayle, A. J.; Berquist, Z. J.; Chen, Y.; Hill, A. J.; Hoffman, J. Y.; Bielinski, A. R.; Lenert, A.; Dasgupta, N. P. Tunable Atomic Layer Deposition into Ultra-High-Aspect-Ratio (>60000:1) Aerogel Monoliths Enabled by Transport Modeling. *Chem. Mater.* **2021**, *33*, 5572−5583.
(66) Chung, J.; Myoung, J.; Oh, J.; Lim, S. Synthesis of a ZnS Shell on the ZnO Nanowire and Its Effect on the Nanowire-Based Dye-Sensitized Solar Cells. *J. Phys. Chem. C* **2010**, *114*, 21360−21365.
(67) Parsons, G. N.; Clark, R. D. Area-Selective Deposition: Fundamentals, Applications, and Future Outlook. *Chem. Mater.* **2020**, *32*, 4920−4953.
(68) Cho, T. H.; Farjam, N.; Allemang, C. R.; Pannier, C. P.; Kazyak, E.; Huber, C.; Rose, M.; Trejo, O.; Peterson, R. L.; Barton, K.; Dasgupta, N. P. Area-Selective Atomic Layer Deposition Patterned by Electrohydrodynamic Jet Printing for Additive Manufacturing of Functional Materials and Devices. *ACS Nano* **2020**, *14*, 17262−17272.
(69) Liu, Y.; Liu, M.; Swihart, M. T. Plasmonic Copper Sulfide-Based Materials: A Brief Introduction to Their Synthesis, Doping, Alloying, and Applications. *J. Phys. Chem. C* **2017**, *121*, 13435−13447.
(70) Wagner, R.; Wiemhöfer, H.-D. Hall Effect and Conductivity in Thin Films of Low Temperature Chalcocite Cu_2S at 20 °C as a Function of Stoichiometry. *J. Phys. Chem. Solids* **1983**, *44*, 801−805.
(71) Johansson, J.; Kostamo, J.; Karppinen, M.; Niinistö, L. Growth of Conductive Copper Sulfide Thin Films by Atomic Layer Deposition. *J. Mater. Chem.* **2002**, *12*, 1022−1026.
(72) Jo, J.; Lenef, J. D.; Mashooq, K.; Trejo, O.; Dasgupta, N. P.; Peterson, R. L. Causes of the Difference Between Hall Mobility and Field-Effect Mobility for p-Type RF Sputtered Cu_2O Thin-Film Transistors. *IEEE Trans. Electron Devices* **2020**, *67*, 5557−5563.

https://doi.org/10.1021/acs.chemmater.2c03773
Chem. Mater. 2023, 35, 2503−2517